sensors

MDPI

Article

Achievement of High-Response Organic Field-Effect Transistor NO_2 Sensor by Using the Synergistic Effect of ZnO/PMMA Hybrid Dielectric and CuPc/Pentacene Heterojunction

Shijiao Han [1], Jiang Cheng [2], Huidong Fan [1], Junsheng Yu [1,2,*] and Lu Li [2,*]

[1] State Key Laboratory of Electronic Thin Films and Integrated Devices, School of Optoelectronic Information, University of Electronic Science and Technology of China (UESTC), Chengdu 610054, China; 201211050108@std.uestc.edu.cn (S.H.); 201511050103@std.uestc.edu.cn (H.F.)

[2] Co-Innovation Center for Micro/Nano Optoelectronic Materials and Devices, Research Institute for New Materials and Technology, Chongqing University of Arts and Sciences, Chongqing 402160, China; caiwu0301@163.com

* Correspondence: jsyu@uestc.edu.cn (J.Y.); lli@cqwu.edu.cn (L.L.); Tel.: +86-28-8320-7157 (J.Y.); +86-23-4951-2058 (L.L.)

Academic Editors: Eduard Llobet and Stella Vallejos
Received: 10 August 2016; Accepted: 18 October 2016; Published: 21 October 2016

Abstract: High-response organic field-effect transistor (OFET)-based NO_2 sensors were fabricated using the synergistic effect the synergistic effect of zinc oxide/poly(methyl methacrylate) (ZnO/PMMA) hybrid dielectric and CuPc/Pentacene heterojunction. Compared with the OFET sensors without synergistic effect, the fabricated OFET sensors showed a remarkable shift of saturation current, field-effect mobility and threshold voltage when exposed to various concentrations of NO_2 analyte. Moreover, after being stored in atmosphere for 30 days, the variation of saturation current increased more than 10 folds at 0.5 ppm NO_2. By analyzing the electrical characteristics, and the morphologies of organic semiconductor films of the OFET-based sensors, the performance enhancement was ascribed to the synergistic effect of the dielectric and organic semiconductor. The ZnO nanoparticles on PMMA dielectric surface decreased the grain size of pentacene formed on hybrid dielectric, facilitating the diffusion of CuPc molecules into the grain boundary of pentacene and the approach towards the conducting channel of OFET. Hence, NO_2 molecules could interact with CuPc and ZnO nanoparticles at the interface of dielectric and organic semiconductor. Our results provided a promising strategy for the design of high performance OFET-based NO_2 sensors in future electronic nose and environment monitoring.

Keywords: NO_2 sensors; organic field-effect transistor (OFET); synergistic effect; ZnO/PMMA hybrid dielectric; heterojunction structure

1. Introduction

Since air pollution has become an urgent global problem with the development of industry and technology, detecting gases, especially toxic gases, as the basis for controlling air pollution, has become increasingly significant [1]. One of the most common and detrimental air pollutant oxidizing gases is nitrogen oxides, including nitrogen dioxide (NO_2), which is produced and released into atmosphere from combustion and automotive emission. In addition to contributing to the formation of fine particle pollution, NO_2 is linked with a number of adverse effects on the respiratory system such as chronic bronchitis, emphysema, and respiratory irritation at low concentrations [2–4]. The potential detrimental impact of NO_2 emission on public health and the environment has led to extensive scientific and

technological progress in the field of NO_2 sensors. Therefore, many NO_2 sensors are commercially available, such as electrochemical, resistive, and optical sensors [5,6]. Optical methods, which rely on the unique optical fingerprints of NO_2 gas molecules, have the highest sensitivity despite their sizes and costs [7]. Electrochemical sensing mainly depends on electrochemical reduction between NO_2 and catalysts, which is low-cost but has a short lifetime [8]. NO_2 sensing based on resistive relies on the charge transfer between metal oxides and NO_2 absorbed on the surface, which has poor selectivity and needs high temperature to achieve recovery or reaction [9]. However, with the development of two-dimensional (2D) materials, Ou et al. have realized selective and reversible NO_2 gas sensing by using the charge transfer between physisorbed NO_2 gas molecules and 2D tin disulfide (SnS_2) and molybdenum disulfide (MoS_2) at low operating temperatures [10,11].

As a new developing sensing platform, organic field-effect transistor (OFET)-based sensors have attracted intriguing attention owing to their advantages of plenty organic material resources, mechanical flexibility, and microarray compatibility [12,13]. As a key functional layer of an OFET-based sensor, organic semiconductor (OSC) materials have become promising candidates for gas sensors due to their high sensitivity, low production costs, and room temperature detection [14,15]. Mostly, the efforts involved in developing a high performance OFET-based gas sensor are mainly focused on the OSC layers [16]. However, the interface property of dielectrics also plays a crucial role in the gas sensing characteristics, as the efficient current channel lies in the first few molecular layers of the OSC upon the dielectric layer [17]. Using scanning Kelvin probe microscopy, Andringa et al. have determined that the trapped electrons of OFET-based sensors are located at the dielectric interface [18]. Therefore, modifying dielectrics with certain functional materials could significantly improve the sensing properties of OFET-based chemical sensors.

Furthermore, great efforts in device engineering of OFETs have been made to construct a series of sensing devices with high selectivity, one of the most efficient methods is to implant functional receptors [14]. Specifically, metal phthalocyanines (MPc) molecules have low ionization energy, which imparts low activation energy for the formation of charge transfer complexes with oxidizing gases [13]. NO_2 is a strong-binding gaseous oxidant, so MPc films have been widely used in NO_2 detection, such as copper(II) phthalocyanine (CuPc), titanyl phthalocyanine (TiOPc) and hexadecafluorinated copper phthalocyanine (F16CuPc) [19]. Yan et al. reported a TiOPc/F16CuPc heterojunction gas sensor with an enhanced relative response to NO_2 as low as 5 ppm and a detection limit down to 250 ppb at room temperature [20]. By adding a highly sensitive vanadyl phthalocyanine (VOPc) layer on top of the single heterojunction device to form a double heterojunction, the relative-response intensity could be improved significantly [21]. This result indicated that using a MPc ultrathin heterojunction can present a high response NO_2 gas sensor, which makes it very promising in the low-cost room-temperature-sensor area. As our previous research shows, zinc oxide (ZnO) nanoparticles at the OSC/dielectric interface would decrease the grain size of OSC deposited on the hybrid dielectric, and, meanwhile, the boundary between crystals was increased [22]. More notably, ZnO and related nanostuctures, suh as NO_2 sensible materials, have extensively been used in resistance and field-effect transistor-based NO_2 sensors [23–25]. However, the work on the use of synergistic effect of ZnO nanoparticles and CuPc/pentacene heterojunction to enhance the relative response of the OFET-based gas sensors was rarely reported. Therefore, our research can develop a new strategy to realize the high relative response commercial OTFT-based gas sensors.

In this work, we used the synergistic effect of zinc oxide/poly(methyl methacrylate) (ZnO/PMMA) hybrid dielectric and CuPc/pentacene heterojunction to realize high sensitivity OFET-based NO_2 gas sensors. The ZnO/PMMA hybrid dielectric was fabricated by simply blending the ZnO nanoparticles and PMMA solutions, and the heterojunction was formed by adding an ultrathin CuPc layer on the top of pentacene. The synergistic effect of hybrid dielectric and organic semiconductor layers was characterized by the control experiments. Moreover, the selectivity and stability of this OFET-based gas sensor were characterized in detail. The results of this research may improve our understanding of design strategy for OFET-based gas sensors.

2. Materials and Methods

2.1. ZnO/PMMA Hybrid Preparation

ZnO nanoparticles were prepared according to the method reported in the previous literature [26], and the average size of as-synthesized quasispherical ZnO NPs was 4.9 nm. ZnO nanoparticles were divided from methanol by centrifugation and dispersed in chloroform/methanol (50 mL, v/v = 90:10) to obtain a stock solution. PMMA (average molecules weight ~120,000) was dissolved in anisole with a concentration of 200 mg/ml. The obtained solution was mixed with the prepared ZnO nanoparticles dispersion (v/v = 1:1). The ZnO/PMMA hybrid dielectric was fabricated using spin coating process.

2.2. Device Preparation

Figure 1 shows the molecular structures of pentacene, CuPc and PMMA and schematic structure of the top-contacted OFET-based sensors with only CuPc/pentacene heterojunction (device A) and both ZnO/PMMA hybrid dielectric and CuPc/pentacene heterojunction (device B). The OFETs were processed according to the following procedure. Indium tin oxide (ITO) coated glass was used as substrate and gate electrodes. Prior to the spin-coating of the dielectric layers, the substrates were successively ultrasonically cleaned in acetone, deionized water and isopropyl alcohol. ZnO/PMMA hybrid and PMMA, functioned as the gate dielectric, were spin-coated on ITO substrate at room temperature (25 °C) and baked in an oven at 90 °C for 2 h. Subsequently, 30 nm pentacene and 5 nm thick CuPc were thermally evaporated in a vacuum of ~2×10^{-4} Pa at a rate of 0.2 Å/s successively. Finally, the source and drain electrodes of 50 nm gold (Au) were thermally deposited using a shadow mask at a rate of 10 Å/s. The length and width of the channel were 100 μm and 1 cm, respectively.

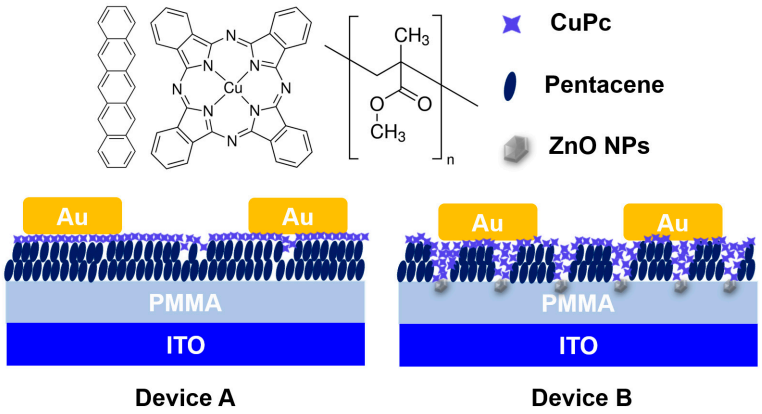

Figure 1. Molecular structures of the pentacene, CuPc and PMMA, along with the organic field-effect transistor (OFET)-based sensor device configurations in this study, device A with only CuPc/Pentacene heterojunction; device B with both ZnO/PMMA hybrid dielectric and CuPc/Pentacene heterojunction.

2.3. Device Test and Data Analyses

The electrical characteristics of all the devices were measured with a Keithley 4200 sourcemeter (Tektronix, Shanghai, China) under ambient conditions at room temperature.

The morphologies of the organic semiconductor were characterized with atomic force microscopy (AFM) (Agilent, AFM 5500) in a tapping mode. The OFET sensor was stored in an airtight test chamber (approximately 0.02 L). Dry air and 100 ppm standard NO_2 gases (anhydrous) were purchased from Sichuan Tianyi Science and Technology Co., Chengdu, China, and a mixture with the appropriate concentration was introduced into the test chamber by a mass flow controller (S48 300/HMT, Beijing Boriba Metron Instruments Co., Beijing, China). NO_2 gas response characteristics of the OFET sensors were measured with a variation of drain-source current, which acted as a function of time. Also, the transfer curves in various concentrations of NO_2 were systematically characterized.

The field-effect mobility of device was extracted in the saturation regime from the highest slope of $|I_{DS}|^{1/2}$ vs. V_G plots by using Equation (1):

$$I_{DS} = (\frac{WC_i}{2L})\mu(V_G - V_T)^2 \quad (1)$$

where L and W are the channel length and width, respectively. C_i is the capacitance (per unit area) of the dielectric, V_G is the gate voltage, and I_{DS} is the drain-source current.

3. Results and Discussion

Figure 2 depicts the representative transfer plots of devices A and B. Both devices A and B have the typical behavior of a p-type transistor. Device A exhibits a field-effect mobility (μ), a current on/off ratio (I_{on}/I_{off}), a threshold-voltage (V_T), and a sub-threshold slope(SS) of 0.13 $cm^2 \cdot V^{-1} \cdot s^{-1}$, 2.0×10^3, -12 V, and 3.0 V/dec, respectively. In contrast, the values of μ, I_{on}/I_{off}, V_T, and SS for device B are 0.006 $cm^2 \cdot V^{-1} \cdot s^{-1}$, 8.9×10^1, -15 V and 15 V/dec, respectively. It is obvious that the device performance of CuPc/pentacene heterojunction OFETs based on pure PMMA is much higher than that of based on ZnO/PMMA hybrid dielectric. Compared with our previous results [22], ZnO nanoparticles can lead to more serious performance decrease on CuPc/pentacene heterojunction-based device than the pentacene-based device. This phenomenon indicates that CuPc may also play an essential role as well as ZnO nanoparticles, i.e., they have a synergistic effect.

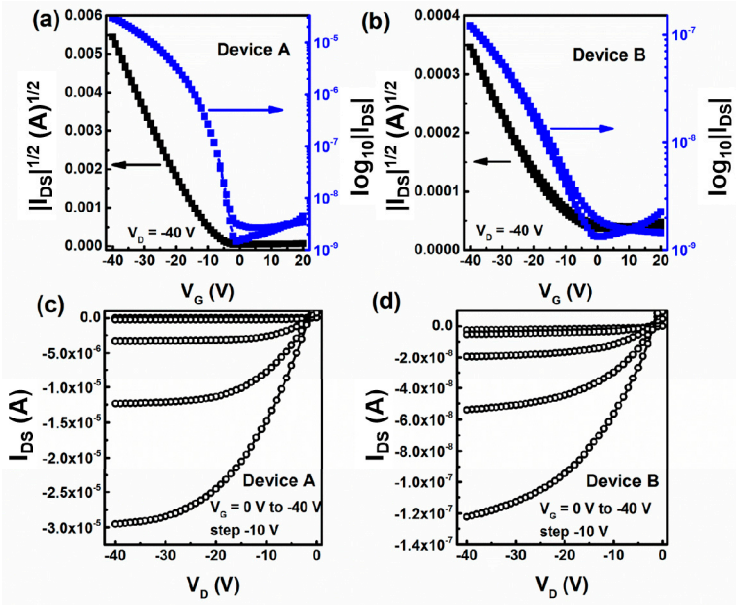

Figure 2. (**a**,**b**) Typical transfer curve I_{DS}-V_G, and (**c**,**d**) output curve I_{DS}-V_D of devices A and B, respectively.

Then, the OFETs were exposed to NO_2 atmosphere with various concentrations that ranged from 0 to 15 ppm. All the devices were exposed to a specific concentration of NO_2 for 5 min before measuring. The gate voltage V_G was from 20 to -40 V and the drain voltage V_D was -40 V. As shown in Figure 3, the curves of device A exhibit a slight shift, but that of device B shifts more significantly.

To intuitively illuminate sensing property, several parameters were calculated from the transfer curve to evaluate the performance of OFET sensors, such as I_{on}, μ, V_T, and SS. The variation of multiple parameters defined as $\Delta R = (R_{NO2} - R_{AIR})/R_{AIR} \times 100\%$ is presented in Figure 4. As shown in Figure 4a,b, the variations of I_{on} and μ of device A and device B show an opposite trend along with the increasing concentration of NO_2, the I_{on} and μ of device B increase by 193% and 69% at 15 ppm NO_2, while that of device A decreases by 30% and 28%. Since the I_{on} and μ of pentacene-based

OFETs will increase significantly when exposed to NO_2 atmosphere [17], CuPc might have a different impact on devices A and B. The V_T of device B presents a remarkable decrease about 80%, while that of device A shows nearly no change. Because V_T is usually referred to charge trapping at the dielectric/semiconductor interface, the more hole charges trap at the interface, the stronger negative gate voltage is needed to turn the transistor on, and vice versa. Thus, the dielectric/semiconductor interface of device A has less trap sites than device B after being exposed to NO_2, and the NO_2 interact places do not locate at this interface.

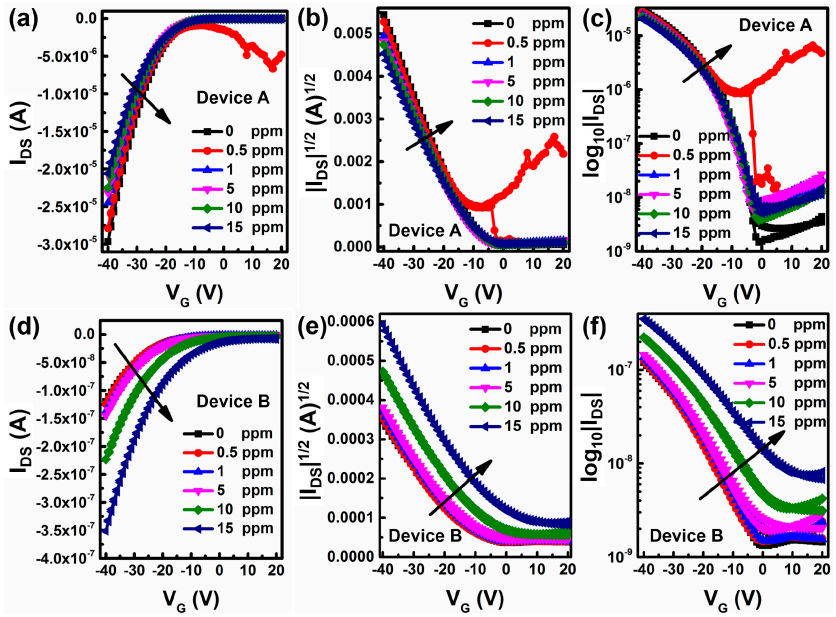

Figure 3. Transfer curves of devices A and B under a specific concentration of NO_2, (**a**,**d**) without calculation, (**b**,**e**) after taking log, (**c**,**f**) after extracting.

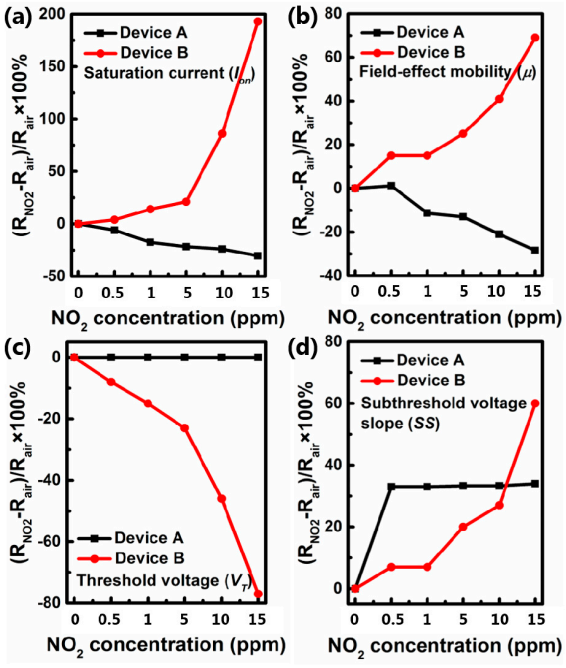

Figure 4. Percentage variation of I_{on} (**a**), μ (**b**), V_T (**c**) and SS (**d**) of all the devices at different NO_2 concentrations, respectively.

Furthermore, *SS* is proportional to the trap density at the interface of dielectric and organic semiconductor, and the trap density (N) can be extracted by Equation (2):

$$SS = \frac{kT}{q}\log_{10}(1 + \frac{qN}{C})^2 \quad (2)$$

where q is the electronic charge, k is Boltzmann's constant, T is absolute temperature, and C is the areal capacitance of the dielectric structure. So the *SS* is proportional to the *N*. As shown in Figure 4d, the *SS* increases constantly to 60% in device B at 15 ppm NO_2 concentration. Nevertheless, the SS of device A is almost unchanged under the concentration of 0.5–15 ppm NO_2. So the interaction in device A between NO_2 and dielectric/organic semiconductor interface is different from that of device B.

To study the reason for the deviation in sensing performance, AFM was utilized to observe the morphologies of active films (AFM images of dielectrics are shown in Figure S1). As shown in Figure 5a,b, the grain size of pentacene in device B is much smaller than that in device A, indicating that ZnO nanoparticles embedded in PMMA dielectric act as impurities and influence the morphology of pentacene film by three aspects: decreasing the grain size, deepening the grain boundary, and disordering molecular arrangement [27]. From Figure 5c, it can be clearly observed that the ultrathin film of CuPc in device B forms a relatively homogeneous film.

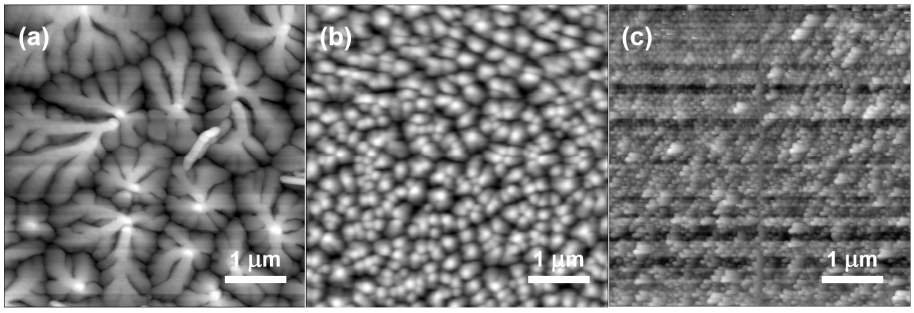

Figure 5. Atomic force microscopy (AFM) topography images of the pentacene films on pure PMMA dielectric (**a**); ZnO/PMMA hybrid dielectrics (**b**) and CuPc film on it (**c**).

From the above discussion, it can be deduced that the enhancement of the sensing properties is attributed to the synergistic effect of ZnO/PMMA hybrid dielectric and CuPc/pentacene heterojunction: (1) ZnO nanoparticles embedded in PMMA will dramatically decrease the grain size and enlarge the depth of grain boundary, which not only increases the potential barrier but also makes the subsequent CuPc molecules partially diffuse into the interface of pentacene and hybrid dielectric. Moreover, the nitrogen atoms around the Cu atom have a relatively high electron density, which can act as hole-charge traps. Thus, the I_{on} and μ of device B are much lower than those of device A; (2) When device B is exposed to NO_2, as shown in Figure 6, NO_2 can diffuse directly into the interface of organic semiconductor and hybrid dielectric, then interact with ZnO nanoparticles and CuPc. As is well known, NO_2 is a strong oxidizing gas with very high electron affinity, so it will interact with the surface of ZnO nanoparticles through surface-adsorbed oxygen ions [23]. Similarly, CuPc molecules can interact with NO_2 and form charge complex due to the delocalized π-electrons which are readily ionized [13]. NO_2 can weaken the impact of ZnO nanoparticles and CuPc at or near the dielectric/organic semiconductor interface on charge transport effectively, so I_{on}, μ and V_T are significantly improved. As a result, the high relative responses can be achieved. The main difference between devices A and B is that CuPc affects the charge conducting channel directly as a functional receptor under the action of ZnO nanoparticles. Device A just forms a simple vertical heterojunction; the sensing mechanism is dependent on the energy level disordering after being exposed to NO_2. Because the NO_2-induced domain fracture originates at the CuPc/Au interface, it is proposed that the NO_2-induced domain fraction also degrades the CuPc/Au electrical contacts, the increased density

of domain boundaries would therefore act to trap carriers near the contacts and induce positive uncompensated charge, which is consistent with the decrease of I_{on} [13].

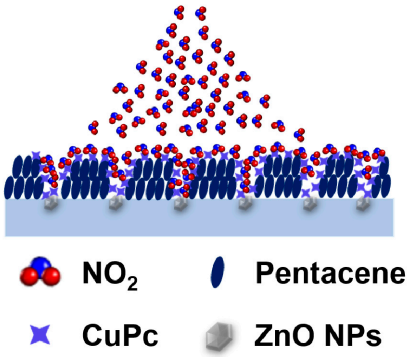

Figure 6. Schematic illustration of ZnO/PMMA hybrid dielectric and CuPc/pentacene heterojunction under NO_2.

The real-time response curve of device B for NO_2 detection was also studied (Figure 7). The pulse of each NO_2 concentration was 10 min. During the recovery process, NO_2 gas was removed, and the sensor was exposed to dry air for 10 min. It is obvious that, when exposed to different NO_2 concentrations, device B has a fast response.

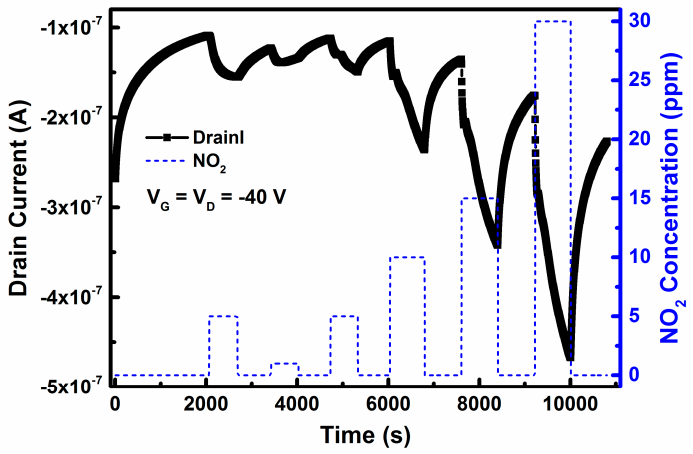

Figure 7. Real-time response curve of this OFET sensor based on ZnO/PMMA hybrid dielectric and CuPc/pentacene heterojunction to different NO_2 pluses.

In addition to the response of fresh OFET sensor, the environmental stability under ambient atmosphere is of critical importance to the practical application of OFET-based sensors and the overall lifetime of the device [28,29]. Thus, the sensor that was tested was stored in ambient air with a relative humidity of ~50% for 30 days, the testing process was similar to the aforementioned fresh device characterization. The variation of its output current at $V_G = -40$ V when exposed to different NO_2 concentrations (ranging from 0.5 to 15 ppm) is shown in Figure 8a. As shown in Figure 8b, the relative change of I_{on} at 0.5 ppm NO_2 is more than 10 times higher than that of the fresh device (more than twice at 15 ppm). Moreover, after being exposed to 15 ppm NO_2, the device still can detect 0.5 ppm NO_2 effectively, and exhibit a high stability to constantly detection. As lots of H_2O and O_2 is absorbed on the surface of ZnO nanoparticles, a large enhancement of sensitivity may be attributed to the concerted efforts of H_2O, O_2 and NO_2 [30–32].

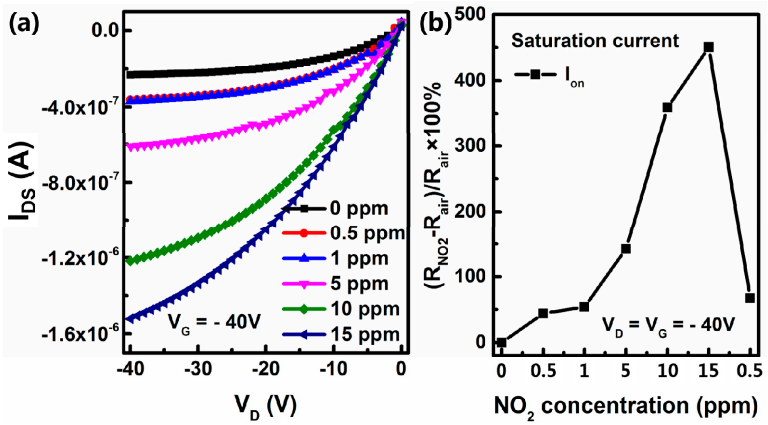

Figure 8. Output curve of devices B (**a**) and percentage variation of I_{on} (**b**) under a specific concentration of NO_2 after stored under ambient for 30 days.

Selectivity is a crucial parameter and an open issue for practical sensing applications, which usually relies on the specific interaction or energy modulation between the organic semiconductors and the analytes [33,34]. Another common kind of air pollutant oxidizing gas of sulfur oxides, sulfur dioxide (SO_2) was also investigated by using device B. As shown in Figure 9, the V_T increases and the I_{on} decreases along with the increase of SO_2 concentration. Surprisingly, this result is opposite to the conventional phenomenon of oxidizing gases [35]. This result may be due to the interaction between ZnO and SO_2 at room temperature, yielding SO_4^{2-}, which can act as the hole trap sites at the interface of dielectric and organic semiconductor [36,37].

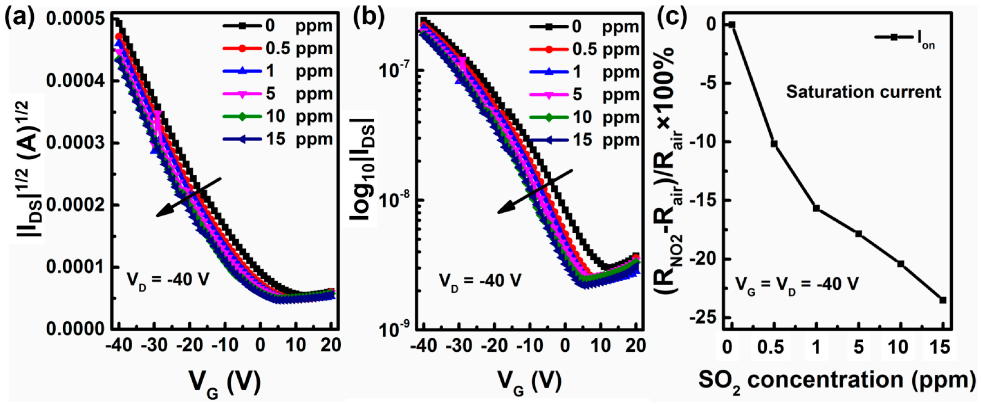

Figure 9. Transfer curves of devices B (**a**,**b**) and percentage variations of I_{on} (**c**) under a specific concentration of SO_2.

4. Conclusions

In conclusion, the ZnO/PMMA hybrid dielectric and CuPc/pentacene heterojunction were used to achieve a high response OFET-based NO_2 gas sensor, exhibiting a dramatic variation of I_{on}, μ, and V_T after being exposed to NO_2. The I_{on} and V_T increased by 193% and 77% at 15 ppm NO_2, and by 5% and 8% at 0.5 ppm NO_2. Moreover, after storing at atmosphere for 30 days, the relative change of I_{on} at 0.5 ppm NO_2 was more than 10 times higher (about 50%) than that of a fresh device. The high performance of this OFET-based sensor was attributed to the synergistic effect of ZnO/PMMA hybrid dielectric and CuPc/pentacene heterojunction. In addition, the sensor with synergistic effect could clearly distinguish the oxidizing gas of NO_2 from SO_2 with opposite I_{on} variation. Using the synergistic effect of dielectric and organic semiconductor is demonstrated to be an effective method for device engineering in OFET-based gas sensors.

Supplementary Materials: The supplementary materials can be found at http://www.mdpi.com/1424-8220/16/10/1763/s1.

Acknowledgments: This research was funded by the National Natural Science Foundation of China (NSFC) (Grant Nos. 61675041, 61505018, 51503022) and the Foundation for Innovation Research Groups of the National Natural Science Foundation of China (Grant No. 61421002). Also, this work was sponsored by Science & Technology Department of Sichuan Province via Grant No. 2016HH0027.

Author Contributions: Shijiao Han conceived and designed the experiments, and wrote the manuscript; Huidong Fan performed the experiments; Shijiao Han and Jiang Cheng analyzed the data; Lu Li contributed part of reagents/materials/analysis tools; Prof. Junsheng Yu is the supervisor of the first author. All authors read and approve the final manuscript.

Conflicts of Interest: The authors declare no conflict of interest.

References

1. Zhang, H.; Li, Q.; Huang, J.; Du, Y.; Ruan, S.C. Reduced graphene oxide/Au nanocomposite for NO_2 sensing at low operating temperature. *Sensors* **2016**, *16*, 1152. [CrossRef] [PubMed]
2. Long, H.; Harley-Trochimczyk, A.; Pham, T.; Tang, Z.; Shi, T.; Zettl, A.; Carraro, C.; Worsley, M.A.; Maboudian, R. High surface area MoS_2/graphene hybrid aerogel for ultrasensitive NO_2 detection. *Adv. Funct. Mater.* **2016**, *26*, 5158–5165. [CrossRef]
3. Jalil, A.R.; Chang, H.; Bandari, V.K.; Robaschik, P.; Zhang, J.; Siles, P.F.; Li, G.; Bürger, D.; Grimm, D.; Liu, X.; et al. Fully integrated organic nanocrystal diode as high performance room temperature NO_2 sensor. *Adv. Mater.* **2016**, *28*, 2971–2977. [CrossRef] [PubMed]
4. Shi, W.; Yu, X.; Zhang, Y.; Yu, J. DNA based chemical sensor for the detection of nitrogen dioxide enabled by organic field-effect transistor. *Sens. Actuators B Chem.* **2016**, *222*, 1003–1011. [CrossRef]
5. Wojtas, J.; Mikolajczyk, J.; Bielecki, Z. Aspects of the application of cavity enhanced spectroscopy to nitrogen oxides detection. *Sensors* **2013**, *13*, 7570–7598. [CrossRef] [PubMed]
6. Kuberský, P.; Altšmíd, J.; Hamáček, A.; Nešpůrek, S.; Zmeškal, O. An electrochemical NO_2 sensor based on ionic liquid: Influence of the morphology of the polymer electrolyte on sensor sensitivity. *Sensors* **2015**, *15*, 28421–28434. [CrossRef] [PubMed]
7. Wang, X.D.; Wolfbeis, O.S. Fiber-optic chemical sensors and biosensors. *Anal. Chem.* **2013**, *85*, 487–508. [CrossRef] [PubMed]
8. Shao, Y.; Wang, J.; Wu, H.; Jun Liu, J.; Aksay, I.A.; Lin, Y. Graphene Based electrochemical sensors and biosensors: A review. *Electroanalysis* **2010**, *22*, 1027–1036. [CrossRef]
9. Miller, D.R.; Akbar, S.A.; Morris, P.A. Nanoscale metal oxide-based heterojunctions for gas sensing: A review. *Sens. Actuators B Chem.* **2014**, *204*, 250–272. [CrossRef]
10. Ou, J.Z.; Ge, W.; Carey, B.; Daeneke, T.; Rotbart, A.; Shan, W.; Wang, Y.; Fu, Z.; Chrimes, A.F.; Wlodarski, W.; et al. Physisorption-based charge transfer in two-dimensional SnS_2 for selective and reversible NO_2 gas sensing. *ACS Nano* **2015**, *9*, 10313–10323. [CrossRef] [PubMed]
11. Berean, K.J.; Ou, J.Z.; Daeneke, T.; Carey, B.J.; Nguyen, E.P.; Wang, Y.; Russo, S.P.; Kaner, R.B.; Kalantar-zadeh, K. 2D MoS_2 PDMS Nanocomposites for NO_2 Separation. *Small* **2015**, *11*, 5035–5040. [CrossRef] [PubMed]
12. Yu, J.; Yu, X.; Zhang, L.; Zeng, H. Ammonia gas sensor based on pentacene organic field-effect transistor. *Sens. Actuators B Chem.* **2012**, *173*, 133–138. [CrossRef]
13. Han, S.; Zhuang, X.; Shi, W.; Yang, X.; Li, L.; Yu, J. Poly (3-hexylthiophene)/polystyrene (P3HT/PS) blends based organic field-effect transistor ammonia gas sensor. *Sens. Actuators B Chem.* **2016**, *225*, 10–15. [CrossRef]
14. Huang, W.; Yu, J.; Yu, X.; Shi, W. Polymer dielectric layer functionality in organic field-effect transistor based ammonia gas sensor. *Org. Electron.* **2013**, *14*, 3453–3459. [CrossRef]
15. Zang, Y.; Huang, D.; Di, C.; Zhu, D. Device engineered organic transistors for flexible sensing applications. *Adv. Mater.* **2016**, *28*, 4549–4555. [CrossRef] [PubMed]
16. Mirza, M.; Wang, J.; Wang, L.; He, J.; Jiang, C. Response enhancement mechanism of NO_2 gas sensing in ultrathin pentacene field-effect transistors. *Org. Electron.* **2015**, *24*, 96–100. [CrossRef]
17. Andringa, A.M.; Roelofs, W.S.C.; Sommer, M.; Thelakkat, M.; Kemerink, M.; Leeuw, D.M. Localizing trapped charge carriers in NO_2 sensors based on organic field-effect transistors. *Appl. Phys. Lett.* **2012**, *101*, 153302. [CrossRef]

18. Park, J.H.; Royer, J.E.; Chagarov, E.; Kaufman-Osborn, T.; Edmonds, M.; Kent, T.; Lee, S.; Trogler, W.C.; Kummel, A.C. Atomic imaging of the irreversible sensing mechanism of NO_2 adsorption on copper phthalocyanine. *J. Am. Chem. Soc.* **2013**, *135*, 14600–14609. [CrossRef] [PubMed]
19. Melville, O.A.; Lessard, B.H.; Bender, T.P. Phthalocyanine-based organic thin-film transistors: A review of recent advances. *ACS Appl. Mater. Interfaces* **2015**, *7*, 13105–13118. [CrossRef] [PubMed]
20. Wang, X.; Ji, S.; Wang, H.; Yan, D. Highly sensitive gas sensor enhanced by tuning the surface potential. *Org. Electron.* **2011**, *12*, 2230–2235. [CrossRef]
21. Ji, S.; Wang, H.; Wang, T.; Yan, D. A High-performance room-temperature NO_2 sensor based on an ultrathin heterojunction film. *Adv. Mater.* **2013**, *25*, 1755–1760. [CrossRef] [PubMed]
22. Han, S.; Huang, W.; Shi, W.; Yu, J. Performance improvement of organic field-effect transistor ammonia gas sensor using ZnO/PMMA hybrid as dielectric layer. *Sens. Actuators B Chem.* **2014**, *203*, 9–16. [CrossRef]
23. Afzal, A.; Cioffi, N.; Sabbatini, L.; Torsi, L. NOx sensors based on semiconducting metal oxide nanostructures: Progress and perspectives. *Sens. Actuators B Chem.* **2012**, *171–172*, 25–42. [CrossRef]
24. Fan, F.; Feng, Y.; Bai, S.; Feng, J.; Chen, A.; Li, D. Synthesis and gas sensing properties to NO_2 of ZnO nanoparticles. *Sens. Actuators B Chem.* **2013**, *185*, 377–382. [CrossRef]
25. Andringa, A.M.; Piliego, C.; Katsouras, I.; Blom, P.W.M.; Leeuw, D.M. NO_2 detection and real-time sensing with field-effect transistors. *Chem. Mater.* **2014**, *26*, 773–785. [CrossRef]
26. Yuan, Z.L.; Yu, J.S.; Wang, N.N.; Jiang, Y.D. A hybrid photodiode with planar heterojunction structure consisting of ZnO nanoparticles and CuPc thin film. *Curr. Appl. Phys.* **2012**, *12*, 1278–1282. [CrossRef]
27. Sun, X.; Liu, Y.; Di, C.A.; Wen, Y.; Guo, Y.; Zhang, L.; Zhao, Y.; Yu, G. Interfacial heterogeneity of surface energy in organic field-effect transistors. *Adv. Mater.* **2011**, *23*, 1009–1014. [CrossRef] [PubMed]
28. Hammock, M.L.; Appleton, A.L.; Schwartz, G.; Mei, J.; Lei, T.; Pei, J.; Bao, Z. Highly stable organic polymer field-effect transistor sensor for selective detection in the marine environment. *Nat. Commun.* **2014**, *5*, 2954.
29. Chen, H.; Dong, S.; Bai, M.; Cheng, N.; Wang, H.; Li, M.; Du, H.; Hu, S.; Yang, Y.; Yang, T.; et al. Solution-processable, low-voltage, and high-performance monolayer field-effect transistors with aqueous stability and high sensitivity. *Adv. Mater.* **2015**, *27*, 2113–2120. [CrossRef] [PubMed]
30. Ye, R.; Baba, M.; Suzuki, K.; Ohishi, Y.; Mori, K. Effects of O_2 and H_2O on electrical characteristics of pentacene thin film transistors. *Thin Solid Films* **2004**, *464–465*, 437–440. [CrossRef]
31. Aguirre, C.M.; Levesque, P.L.; Paillet, M.; Lapointe, F.; St-Antoine, B.C.; Desjardins, P.; Martel, R. The role of the oxygen/water redox couple in suppressing electron conduction in field-effect transistors. *Adv. Mater.* **2009**, *21*, 3087–3091. [CrossRef]
32. Qu, M.; Li, H.; Liu, R.; Zhang, S.L.; Qiu, Z.J. Interaction of bipolaron with the H_2O/O_2 redox couple causes current hysteresis in organic thin-film transistors. *Nat. Commun.* **2014**, *5*, 3185. [CrossRef] [PubMed]
33. Bakera, C.; Laminacka, W.; Gole, J.L. Sensitive and selective detection of H_2S and application in the presence of toluene, benzene, and xylene. *Sens. Actuators B Chem.* **2015**, *212*, 28–34. [CrossRef]
34. Wang, B.; Huynh, T.; Wu, W.; Hayek, N.; Do, T.T.; Cancilla, J.C.; Torrecilla, J.S.; Nahid, M.M.; Colwell, J.M.; Gazit, O.M.; et al. A highly sensitive diketopyrrolopyrrole-based ambipolar transistor for selective detection and discrimination of xylene isomers. *Adv. Mater.* **2016**, *28*, 4012–4018. [CrossRef] [PubMed]
35. Shaymurat, T.; Tang, Q.; Tong, Y.; Dong, L.; Liu, Y. Gas dielectric transistor of CuPc single crystalline nanowire for SO_2 detection down to sub-ppm levels at room temperature. *Adv. Mater.* **2013**, *25*, 2269–2273. [CrossRef] [PubMed]
36. Chaturvedi, S.; Rodriguez, J.A.; Jirsak, T.; Hrbek, J. Surface chemistry of SO_2 on Zn and ZnO: Photoemission and molecular orbital studies. *J. Phys. Chem. B* **1998**, *102*, 7033–7043. [CrossRef]
37. Wu, C.M.; Baltrusaitis, J.; Gillan, E.G.; Grassian, V.H. Sulfur dioxide adsorption on ZnO nanoparticles and nanorods. *J. Phys. Chem. C* **2011**, *115*, 10164–10172. [CrossRef]